Overview of Results from the Large Helical Device

H.Yamada 1) for the LHD experiment group*

1) National Institute for Fusion Science, Toki 509-5292, Japan
* Contributors come from Budker Institute for Nuclear Physics(Russia), Culham Center for Fusion Energy(UK), CIEMAT(Spain), Doshisha Univ., Fukui Univ., The Graduate Univ. for Advanced Studies, Hokkaido Univ., Ishikawa National College of Technology, Japan Atomic Energy Agency, Kurchatov Institute(Russia), Kyoto Institute of Technology, Kyoto Univ., Kyushu Univ., Max-Planck Institut für Plasmaphysik(Germany), Nagano National College of Technology, Nagoya Univ., National Institute for Fusion Science, Oak Ridge National Laboratory(USA), Osaka Univ., Princeton Plasma Physics Laboratory(USA), Shimane Univ., Shizuoka Univ., Tohoku Univ., Tokyo Institute of Technology, Toyama Univ., and Tsukuba Univ.

E-mail contact of main author : hyamada@LHD.nifs.ac.jp

Abstract   The physical understanding of net-current free helical plasmas has progressed in the Large Helical Device (LHD) since the last Fusion Energy Conference in Geneva, 2008. The experimental results from LHD have promoted detailed physical documentation of features specific to net-current-free 3-D helical plasmas as well as complementary to the tokamak approach. The primary heating source is NBI with a heating power of 23 MW, and ECH with 3.7 MW plays an important role in local heating and power modulation in transport studies. The maximum central density has reached $1.2 \times 10^{21} \mathrm{m}^{-3}$ due to the formation of an *Internal Diffusion Barrier* (IDB) at the magnetic field of 2.5 T. The IDB has been maintained for 3 s by refueling with repetitive pellet injection. The plasma with a central ion temperature reaching 5.6 keV exhibits the formation of an *Internal Transport Barrier* (ITB). The ion thermal diffusivity decreases to the level predicted by neoclassical transport. This ITB is accompanied by spontaneous toroidal rotation and an *Impurity Hole* which generates an impurity-free core. *Impurity Hole* is due to a large outward convection of impurities in spite of the negative radial electric field. The magnitude of the Impurity Hole is enhanced in the magnetic configuration with larger helical ripple and for higher Z impurities. Another mechanism to suppress impurity contamination has been identified at the plasma edge with a stochastic magnetic field. A helical system shares common physics issues with tokamaks such as 3-D equilibria, transport in a stochastic magnetic field, plasma response to a *Resonant Magnetic Perturbation* (RMP), divertor physics, and the role of radial electric field and meso-scale structure.

1. Introduction

The Large Helical Device (LHD) is a large-scale heliotron device employing superconducting coils [1]. The advantage of large, robust and stable steady-state plasmas enables exploration of the frontier of a *stellarator/heliotron* concept and detailed documentation of physical processes in plasmas [2]. Since the plasmas in LHD are intrinsically 3-D, multi-dimensional diagnostics with fine temporal and spatial resolution and numerical computation to cope with a real-3-D geometry have been developed. Physical understanding of net-current free helical plasmas has progressed remarkably in LHD since the last Fusion Energy Conference in Geneva, 2008 [3]. This progress in conjunction with parameter extension directly improves the prospect for a helical reactor and also contributes to a sophisticated understanding of tokamak physics which recently requires a 3-D consideration.

In LHD, a pair of superconducting helical coil generates the confining magnetic field in steady-state. The toroidal periodicity, *M,* is 10. The nominal major and minor radii are 3.7 m and 0.64 m, respectively. The toroidal cross section has an elliptic shape and the minor radius is defined as an averaged value. Since three blocks in layers compose a helical coil, the aspect ratio, A_p, can be controlled by changing the current in each block. The radial position of the

magnetic axis, R_{ax}, and the ellipticity of the magnetic flux surfaces, κ, can be control by 3 sets of poloidal coils. Here κ is also defined as the toroidally averaged value. LHD is also equipped with ten pairs of perturbation coils on the top and the bottom of the main body, which generate a *Resonant Magnetic Perturbation* (RMP) with m/n=1/1. The rotational transform, ɩ, which is the inverse of the safety factor, q, has the opposite trend to that in a tokamak. The ɩ value in the standard geometry (R_{ax}=3.6 m, A_p=5.8, κ=1) is 0.3 and 1.4 at the center and the edge, respectively. Therefore the resonance with the RMP is located in the periphery near the normalized minor radius of 0.9. One of highlighted features in the magnetic geometry of LHD is a built-in divertor, which is naturally generated by a pair of helical coils. The cross section is similar to a double-null configuration in a tokamak but rotates poloidally as the toroidal angle changes. It should be noted that the present divertor set-up is open without an active pumping system. The steep change of the rotational transform at the edge causes overlapping of magnetic islands and consequently stochastic field lines bridge the last closed flux surface and 4 divertor legs. Contrasts and similarities of these characteristics to a tokamak are potential guideposts leading to a comprehensive understanding of toroidal plasmas.

The LHD is the large-scale fully superconducting device with a total stored magnetic energy up to 0.77 GJ. The primary heating source is Neutral Beam Injection (NBI) with a total heating power of 23 MW. Two beam lines among three tangential beam lines with negative ion sources (N-NBI) are arranged in the counter clock-wise direction and the other is in the clock-wise direction. These beam lines have the accelerating voltage of 180 keV with a total power of 16 MW. The combination of these beam lines can drive plasma currents up to 100 kA. Although this current is not large compared with the equivalent plasma current that would be necessary to generate the rotational transform at the edge of 1.5 MA, it is capable of tailoring the rotational transform in the core for physics studies. It should be noted that the profile of the rotational transform can be measured by motional-Stark-effect (MSE) spectroscopy in LHD. Another beam line with positive ion sources (P-NBI) is arranged for perpendicular injection with a power of 7 MW and an accelerating voltage of 40 keV which is preferable for ion heating. The well-focused Electron Cyclotron Heating (ECH) with 3.7 MW plays an important role in local heating and power modulation in transport studies.

A helical system does not have hard density limit like a Greenwald density in a tokamak. Indeed, extremely high density beyond 1×10^{21}m^{-3} is accessible at moderate magnetic fields of less than 3 T in LHD [4]. Its steady-state operation has been demonstrated and important related issues on detachment [5], impurity screening and the effect of RMP have been investigated [6]. Confinement improvement in the ion heat loss channel has lead to a central ion temperature of 5.6 keV at a moderate density of 1.6×10^{19}m^{-3}. Momentum transport is improved coincidently with this confinement improvement and a significant outward convection of impurities has been indentified in these high-ion-temperature plasmas [7]. An *Impurity Hole* develops with increase of the gradient of ion temperature and the dependences of the outward convection, to which this *Impurity Hole* is attributed, on helical ripple and impurity mass have been identified [8]. Direct measurement of the electric potential by the Heavy Ion Beam Probe (HIBP) has enabled an estimate of the radial electric field and consequently accurate discussion about the role of neoclassical transport in these peculiar phenomena [9] as well as in the plasma with *Core Electron-Root Confinement* (CERC) [10]. With regard to CERC in the case of central ECH, fluctuations with long distance correlation have been investigated by Electron Cyclotron Emission (ECE) and reflectometry to clarify the relation between meso-scale turbulence and non-local transport [11,12]. The stability and

confinement in the high-β regime up to 5 % have been investigated in detail [13,14], in particular, with the active control of R_{ax} during the discharge [15]. An RMP has been also applied to clarify the physics of the interchange instability and island generation/healing [16]. The topic of ELM, etc. in a tokamak is attracting interest in the stochastic magnetic field. Stochastization of the magnetic flux surfaces has been confirmed, when magnetic shear becomes weak in the vicinity of a rational surface, by the heat pulses from modulated ECH [17]. Physics related to highly energetic particles has been investigated in terms of the ability to confine trapped particles[18], driven Toroidal Alfvén Eigen (TAE) [19] mode and Geodestic Acoustic Mode (GAM) [20]. Last but not least, LHD has provided a good testbed for studies of plasma wall interactions [21,22] and fundamental physical processes [23].

Table I summarizes plasma and operational parameters in the highlighted plasmas in terms of density, ion temperature, β and electron temperature.

TABLE I   PLSMA PARAMETERS ACHIEVED IN HIGHLIGHTED PLASMAS IN LHD

	$T_i(0)$ (keV)	$T_e(0)$ (keV)	$n_e(0)$ (10^{19}m^{-3})	β (%)	τ_E (s)	P_{abs} (MW)	B(T)
High n_e	0.22	0.22	125	1.43	0.039	21.4	2.51
High β	-	0.43	2.3	5.1	0.008	11.9	0.425
High T_i	5.6	3.8	1.6	0.80	0.046	19.1	2.9
High T_e	-	18.9	0.24	0.19	0.043	3.7	2.71

2. Exploration of High Density Operation Scenario

The maximum central density has reached 1.2×10^{21} m^{-3} due to the formation of the *Internal Diffusion Barrier* (IDB) [24] with large heating power (20 MW) at the moderate magnetic field of 2.5 T. Control of detachment is an important issue in the high-density operational scenario whereby the heat load to the divertor can be reduced through enhanced radiation to ensure sustainable steady-state discharges. Normally, in toroidal devices there exists a density threshold above which detachment occurs, but in LHD the plasma often leads to radiative collapse without detachment. Recent work on LHD has shown the addition of an $m/n=1/1$ magnetic island induced by RMP enhances the detachment process by lowering the density threshold for detachment [4].

The central density of 3×10^{20}m^{-3} with a highly peaked density profile is maintained for $35\tau_E$ by feedback control of pellet injection with the heating power of 10 MW. Figure 1 shows the temporal evolution of the discharge. After sequential pellet injection builds up the density initially, the core density begins to
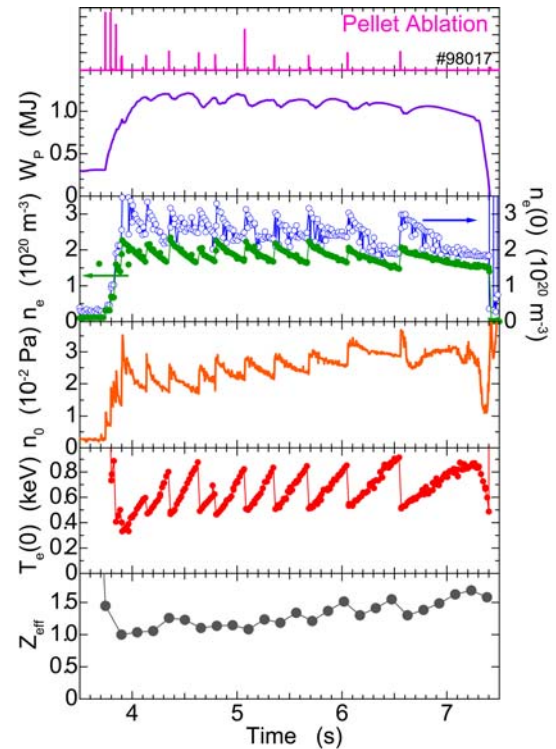

FIG.1 Time traces of the sustainement of the IDB-SDC plasma. From the top, pellet signal, stored energy, center and line-averaged density, neutral pressure, central electron temperature and Zeff.

decrease, while the central electron temperature starts to rise. Then the stored energy develops due to the "reheat" effect, and the *Super Dense Core* (SDC) with an IDB is established. The IDB-SDC phase decays with a time constant of improved particle confinement time without refueling. In

FIG.2 Density profiles at (a) the early phase and (b) later phase of the discharge with an IDB shown in FIG.1.

this discharge, pellets are injected to sustain the IDB-SDC phase with the feedback control of the line integrated density $\bar{n}_e \ell$. This quasi-steady state phase lasts for more than 3 s, which is terminated by switching off the NBIs. Although no serious increase of impurities is observed, the stored energy degrades gradually with the increase of neutral pressure. While the density profile still exhibits an IDB at the end of the discharge, the increase of the density outside IDB becomes pronounced (see *FIG.2*), which indicates an increase of the edge

recycling due to the insufficient pumping capability compared to the supply of particles by pellets. Consequently edge temperature decreases in the later phase and the stored energy degrades. These observations motivate the next-step scenario with improved particle control with the planned closed divertor. An RMP with m/n=1/1, which has resonance in the plasma periphery, has demonstrated the radial expansion of a super-dense-core surrounded by an IDB through the density reduction in the mantle outside the IDB. Also enhancement of the density pump-out by application of the RMP has led to simultaneous achievements of an IDB and detachment.

A mechanism to suppress impurity contamination has been identified as impurity screening at the plasma edge with a stochastic magnetic field [6]. The carbon line emissions reflecting the penetration and source indicates that the screening effect is enhanced by an increase of density (see *FIG.3*). The 3-D simulation of edge plasma by the EMC3[25]-EIRENE[26] code has reproduced experimental observations and clarified the friction-force role in driving the impurities downstream towards the divertor.

The effects of the magnetic island on the 3D radiation structure in attached and detached plasmas have been investigated with the imaging bolometer diagnostics and the simulation by EMC3-EIRENE [5]. This comparative study has concluded that the magnetic island enhances the
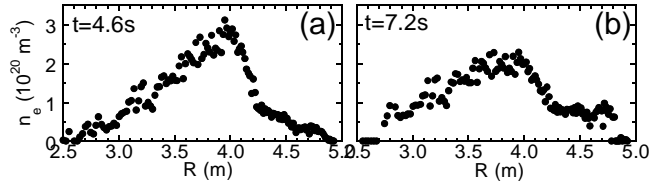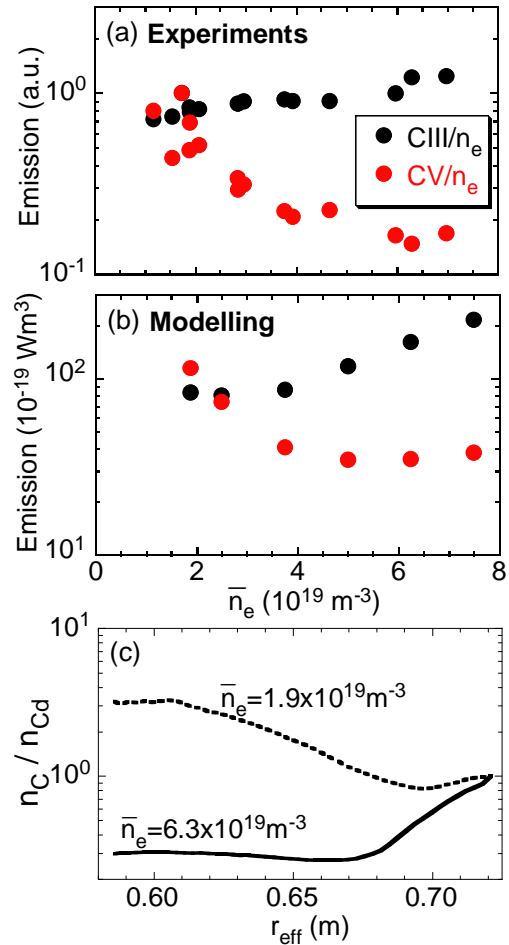

FIG.3 Emissions of CIII (977A) and CV (40.27A) normalized with density as a function of the line-averaged density. (a) Experiment, (b) modelling. The sputtering coefficient is fixed to 2% for all cases. (c) Calculated carbon density profile in the edge plasmas for two typical cases. Carbon density is normalized by that at the dvivetor n_{Cd}

localization of the radiation and is conducive to achieving and sustaining the detachment. With the addition of the magnetic island the carbon radiation profile becomes more localized near the helical divertor x-points. Detachment results in a more asymmetric radiation profile

in the poloidal cross-section with localized peaks near the x-points of the magnetic island as well as the helical divertor. Also the case with the magnetic island exhibits detachment at a lower density than the case without the magnetic island.

3. Characterization of Transport in Improved Confinement

3.1 Thermal Transport

An internal improved mode has been realized in helical plasmas with intensive core heating by ECH. Since the transition of a radial electric field from negative to positive is observed due to the bifurcation of the neoclassical electric field, this improved mode is referred to CERC [27] Also, the plasma with a high central ion temperature exhibits the formation of an *Internal Transport Barrier* (ITB) characterized by peaked temperature and toroidal rotation profiles with steep gradients. In contrast, the radial electric field in the ion ITB core region has been identified as negative by an HIBP. It should be noted that the reduction of anomalous transport in CERC and the ion ITB core is realized where the electric field is positive (neoclassical electron root) and negative (neoclassical ion root), respectively.

Figure 4 shows the growth of the electron temperature profile with CERC [10]. At the beginning of the discharge, a flat T_e profile with a small bump in the core is observed. After that the foot point of this bump moves outward with the increase of $T_e(0)$. Also the gradient of T_e is locally enhanced in the vicinity of the rational surface of $\iota = 1/2$. In contrast, the gradient of T_e between these transport barriers is very small.

With regard to CERC in the case of central ECH, fluctuations with long distance correlation have been investigated at frequencies up to 10 kHz by ECE and reflectometry to clarify the relation between meso-scale turbulence [11] and non-local transport. An analysis of the transient
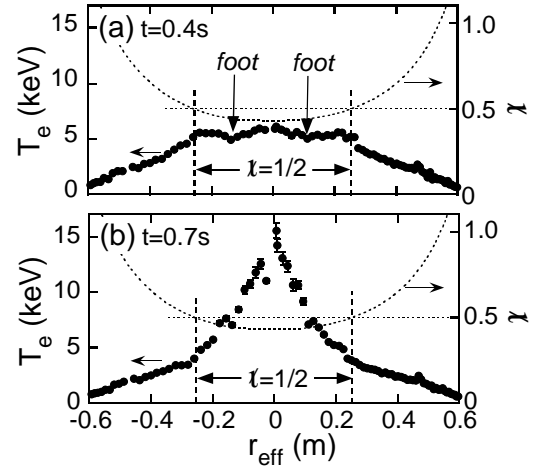
FIG.4 *Temporal development of electron temperature profile in CERC together with the profile of the rotational transform. r_{eff} is the effective minor radius and the negative sign means the torus-inboard side with respect to the magnetic axis.*
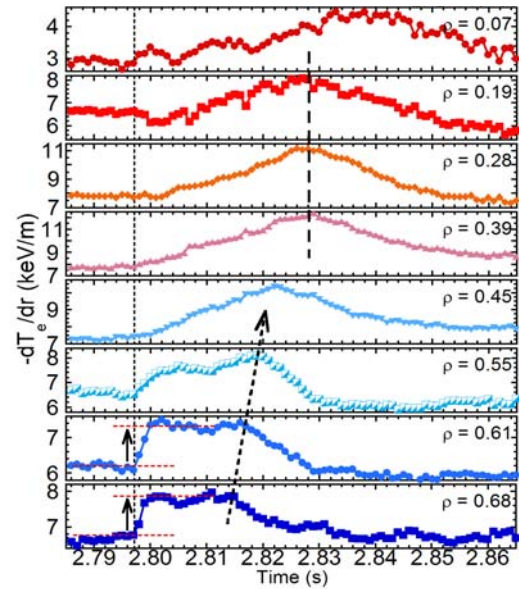
FIG.5 *Temporal evolutions of the electron temperature gradient, which is obtained with the ECE radiometer, at different normalized minor radii in the plasma showing a nonlocal transport phenomenon. All the data is plotted at 1 ms interval. The time of the TESPEL injection is indicated by the vertical short-dashed line.*

response to edge cooling has revealed that the large scale coherent structure connecting the edge and the core regions invokes the nonlocal T_e rise.

Large scale coherent structures in both core and edge regions and their dynamics are clearly observed in a nonlocal transport phenomenon [12]. Figure 5 shows temporal evolutions of the electron temperature gradient $-dT_e/dr$. Right after the injection of a small impurity pellet (TESPEL), the central temperature starts to increase in contrast to the edge cooling. A jump of $-dT_e/dr$ is found to take place in the region extending from $\rho \sim 0.6$ to $\rho \sim 0.7$. Although this $-dT_e/dr$ jump is surely affected by a jump in electron density due to the small impurity pellet injection, the increased $-dT_e/dr$ is sustained for a while unlike the usual case. Thus, a first order transition of electron heat transport, which is categorized by a discontinuity in $-dT_e/dr$, appears over a 6 cm wide region in the periphery. At about the same time, a second order transition of the electron heat transport, which is characterized by a discontinuity in the $d(-dT_e/dr)/dt$, appears over a wide region ($0.28 < \rho \le 0.45$, corresponds to a width of about 10 cm) in the plasma core. These indicate the existence of large scale coherent structures in both core and edge regions, which are of a scale larger than a typical micro-turbulent eddy size (a few mm in this case), and their interaction can cause the nonlocal T_e rise.

In the density decay phase after carbon pellet injection to the plasma heated by both N-NBI and P-NBI with total port-through power beyond 20 MW, the ion and electron temperatures increase with the decrease of electron density. Although the ion ITB has been also observed without carbon pellet injection, the achieved ion temperature with a carbon pellet is higher than that without carbon pellet. The plasma profiles with a typical ion ITB are shown in Fig.6. The central ion temperature of $T_i(0) = 5.6$ keV was achieved with the electron density of $n_e(0) = 1.6 \times 10^{19} \text{m}^{-3}$ and $\bar{n}_e = 1.3 \times 10^{19}$ m^{-3}. The central electron temperature saturated at $T_e(0) \sim 4$ keV and has a broad profile without showing a transport barrier. Tangential NBIs in the co-direction dominate this case and the peaked profile of the toroidal rotation is formed by combination of beam driven rotation and spontaneous rotation in the co-direction as seen in Fig.6(b) [7].

In the phase without the ion ITB, the ion thermal diffusivity is large in the core and roughly scales with gyro-Bohm scaling; $\chi_i \propto T_i^{1.5}$. In the plasma with the ion ITB, the ion thermal diffusivity

FIG.6 Plasma profiles in a typical plasma with an ion ITB. (a) Ion and electron temperatures. (b) Toroidal rotation velocity and electron density.

decreases as the ion temperature increases. The reduction of ion thermal diffusivity with a factor of three has been identified in the core region of the ion ITB plasma. The experimentally obtained ion thermal diffusivity in the ion ITB core is improved to the same level as the neoclassical one, indicating that anomalous transport is significantly reduced.
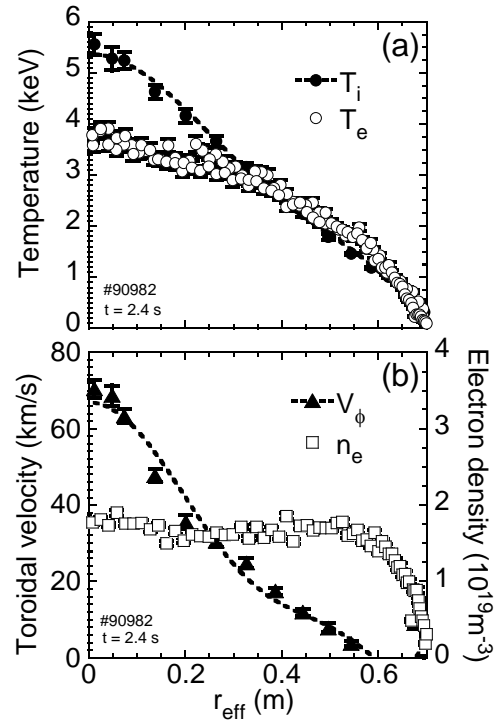
3.2 Role of Off-Diagonal Terms in Momentum and Impurity Transports

As seen in Fig.6(b), the peaked profile of toroidal rotation was observed in the ion ITB core region. The direction of toroidal rotation is determined by momentum input via tangential NBIs. The toroidal rotation velocity and the velocity gradient increase with the torque due to tangential NBIs. The gradient of toroidal velocity also increases with ion temperature gradient. These experimental observations suggest that the improvement of momentum transport occurs when the ion heat transport is improved. In the case without the ion ITB, the gradient of toroidal momentum increases with the radial momentum flux, whereas it increases with an almost constant momentum flux in the case with the ion ITB. The heat diffusivity and the momentum viscosity are compared in Fig.7 and show clear correlation, in which the off-diagonal terms such as intrinsic rotation are not taken in

FIG.7 *Comparison of viscosity against the toroidal rotation and ion thermal diffusivity in the plasmas with an ion ITB.*

account. The absolute value of viscosity is as the same order with the ion thermal diffusivity, that is, Prandtl number($=\mu/\chi_i$) is 0.5-1.0. In addition, the intrinsic rotation in the co-direction driven by the temperature gradient has been identified in the core region [7].
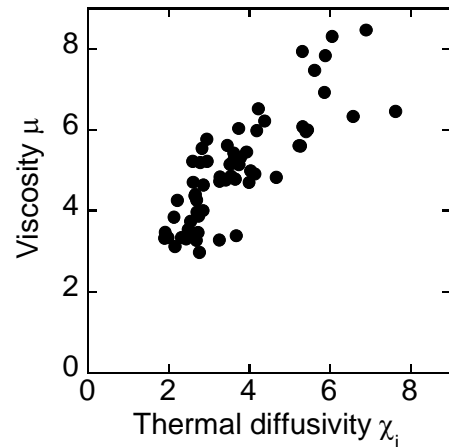
The flux-gradient relation of toroidal rotation shows an offset of momentum transport, indicating the existence of an off-diagonal effect. HIBP measurement has confirmed that the potential gradient (electric field) in the ion ITB core is weakly negative and almost constant during the discharge. The external torque normalized by density monotonically decreases with the ion temperature gradient while the velocity gradient is kept constant. This relation indicates the existence of spontaneous rotation depending on the ion temperature gradient effect in the ion ITB plasmas.

With regard to impurity transport, a favorable mechanism to suppress impurity contamination has been identified. An *Impurity Hole* is derived from an extremely hollow profile of carbon and neon impurities which develops with the increase of the ion temperature gradient [8]. This phenomenon is due to a large outward convection of carbon impurities in spite of the negative radial electric field which has been confirmed by the HIBP. The magnitude of the *Impurity Hole* is enhanced in the magnetic configuration with larger helical ripple and for higher Z (Neon) impurities (see Fig.8).

FIG.8 *Profiles of impurity density normalized by the electron density in plasmas with an ion ITB. Helium, carbon and neon are injected into a plasma intentionally via gas puff or pellet. As Z increases, impurity pump-out is enhanced.*

4. MHD Related Physics

4.1 Exploration of High β Operational Scenario

The operational envelope of high β has been extended in terms of maximum value (the volume
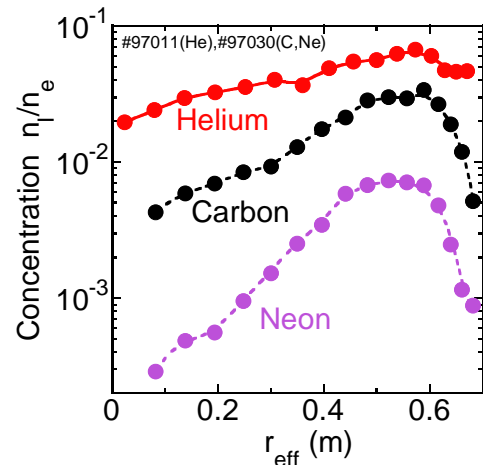
averaged β of 5.1%) as well as duration. The high β state above 4.8 % is maintained stably for $85\tau_E$, which is limited by the capability of NBIs. The optimal high-β operational regime in terms of R_{ax} has been identified by real-time R_{ax} swing, which has contributed to achievement of β of 5.1 %. The precise scan of R_{ax} has indicated that the achievable β has different tendencies for values of lesser R_{ax} and greater R_{ax} than the optimal R_{ax} [15]

Figure 9 shows the achievable β boundary as a function of the vacuum position of R_{ax}. The β limitation by core MHD activity was clearly observed in Region I, where the onset of the low-n MHD mode is qualitatively consistent with the linear theory of the ideal interchange mode. The magnetic geometry impacting the height of a magnetic hill and the strength of magnetic shear can be changed while keeping the pressure

FIG.9 *Achieved volume averaged β as a function of the position of the magnetic axis R_{ax} in vacuum. Several time traces with a dynamical swing of Rax during the discharge are plotted.*

gradient constant which is the driving term of MHD instability. Therefore, the destabilizing thresholds of the geometrical parameter and the pressure gradient have been quantified in the experiment [15]. It should be noted that the observed MHD mode leads to a minor collapse in the core which causes a local flattening of the pressure profile around the resonant surface but does not result in a major collapse. The β degradation in Region II inside the optimal R_{ax} cannot be interpreted by low-n MHD activities. Low-n MHD activities are suppressed in this ideal-stable regime due to spontaneous generation of a magnetic well. The edge instability with $m/n = 2/3$ is observed in Region II but tends to be suppressed by the inward shift of R_{ax}. This low-n mode is a resistive mode. As R_{ax} is shifted inward, this mode is stabilized by the movement of the resonance to the outer region where a pressure gradient is low. The previous high-β experiments indicated that the energy confinement becomes worse with the increase in β. This is due to the increment of the thermal transport in the periphery, which is predicted to be due to resistive-g mode turbulence [14]. The potential reason for the limitation in Region II is enhancement of this turbulence due to the enhancement of the magnetic hill in the periphery by the inward shift of R_{ax}. The boundary in Region III is determined by the general confinement characteristics depending on R_{ax} possibly together with the effect of resistive-g mode turbulence.

4.2 Dynamics of Magnetic Island and Stochacitization

It should be pointed out that 3-D equilibrium has the distinguished features of magnetic islands and stochastic magnetic fields. The characterization of these features encompasses physical topics referred to in this paper. A helical system is intrinsically 3-D, and the finite-β effect and RMP enhance this nature. The bifurcation phenomenon of a magnetic island at a rational surface in LHD suggests that the stochastization of the magnetic surfaces is a self-organized transition phenomenon. Characterization of magnetic islands and stochastic magnetic fields is a common and important issue among toroidal systems. ELM mitigation by means of RMP in a tokamak is a typical and emergent subject. The role of poloidal flows in the dynamics of a magnetic island and stochastization of the magnetic surfaces near a rational surface have been identified experimentally in LHD.
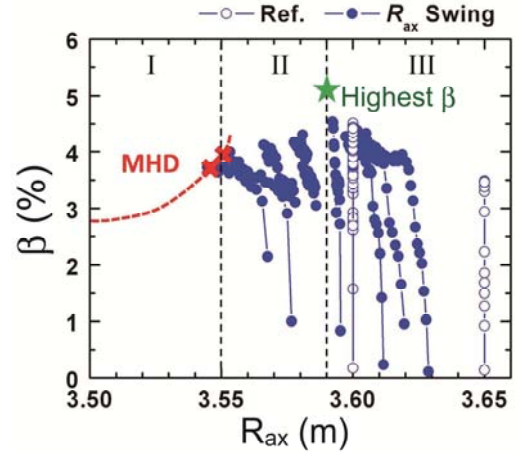
The $m/n=1/1$ island is generated in the peripheral region by an RMP. An earlier work indicated that the generated island is healed below the threshold of collisionality and beyond the threshold of β [28]. The dynamical change of the magnetic island has been investigated in detail by changing the NBI heating power during the discharge with RMP [16]. The temporal increment of the E×B poloidal flow prior to bifurcation from growth to healing of the magnetic island has been observed. Figure 10 shows the correlation between the island growth/healing and the E×B poloidal flow. The direction of the poloidal flow is the electron-diamagnetic direction. From the magnetic diagnostics, it is observed that a resonant current pattern flips by π rad poloidally in the electron-diamagnetic direction during the bifurcation. These experimental observations show

FIG.10 Correlation beween the poloidal flow frequency $\omega_{E×B}$ and the island width evaluated from the local flattening in the electron temperature profile.

that the temporal increment of the poloidal flow is followed by the bifurcation (growth to healing) of the magnetic island and suggests the balance between the viscous drag force due to the poloidal flow and magnetic torque due to an RMP is an important factor to characterize the bifurcation of growth and healing of the magnetic island.
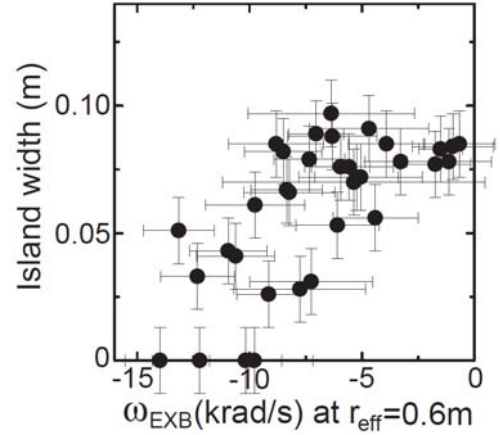
When the arrangement of the tangential NBIs is switched from balanced to counter to equivalent plasma current, the rotational transform even increases due to the return current, although the edge rotational transform increases due to the non-inductive current by neutral beam current drive (NBCD). Then the location of the rational surface of $m/n=2/1$, which corresponds to $\iota = 0.5$, moves toward the magnetic axis and the magnetic shear at a rational surface decreases significantly. When the magnetic shear $(\rho/\iota)d\iota/d\rho$ drops to the critical value (~ 0.5), sudden flattening of the electron temperature profile takes place at the rational surface. The flattening of the temperature profile extends to the plasma center as seen in the drop of electron temperature gradient near the magnetic axis. In this situation, a significant temperature gradient cannot be formed even with the central ECH.

Transport analysis with heat pulses from the modulated ECH has revealed that stochastization of the magnetic flux surfaces causes a flattening of the T_e profile in the vicinity of a rational surface of $m/n=2/1$ [17]. There are significant differences (slow and fast) in the heat pulse propagation at the
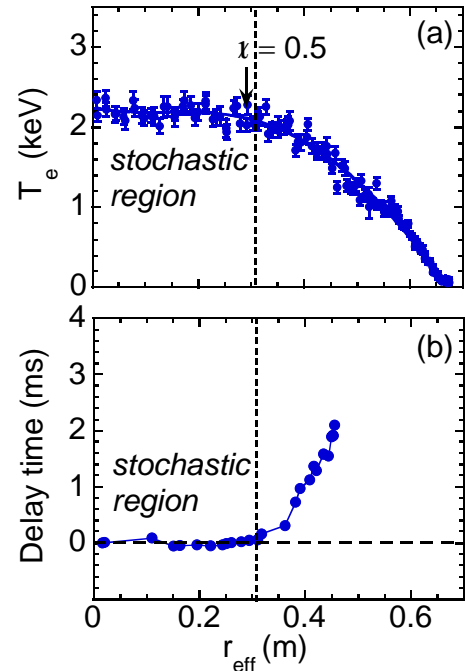

FIG.11 Radial profile of (a) electron temperature and (b) time delay of the heat pulse due to the modulated ECH in the case with stochastic region. The location of rational surface of $\iota = 1/2$ is indicated with an arrow.

flat region of the electron temperature profile between the plasma with medium magnetic shear and weak shear. Slow heat pulse propagation observed in the weak shear is evidence of a nested magnetic island, while the fast heat pulse propagation observed in the plasma with medium magnetic shear is evidence of stochastization of the magnetic surfaces (see FIG.11).

4.3 Mode and Transport Driven by Highly Energetic Particles

Energetic-particle driven Alfvén Eigenmodes(AEs) can enhance the radial transport of energetic particles. A *Geodesic Acoustic Mode* (GAM) driven by energetic particles has been identified by the HIBP diagnostics. The GAM frequency shifts upward in plasmas with monotonic magnetic shear. Electron cyclotron current drive (ECCD) has been used for control of the rotational-transform profile. In plasmas with a reversed magnetic shear, potential fluctuations with a frequency in the same range as the predicted GAM frequency (~30 kHz)

have been observed together with the reversed-shear Alfvén Eigenmode(RSAE) and the analysis of correlated magnetic fluctuations has indicated that the toroidal mode number is zero. The temperature dependence of the frequency is shown in Fig.12, where the ion temperature is much lower than the electron temperature. The observed frequency is proportional to the square-root of the electron temperature, which agrees well with the physics picture of the GAM. Therefore this mode is possibly the GAM. The GAM in the reversed-shear plasma is localized near the magnetic axis. It has been confirmed that the GAM is accompanied by an electrostatic potential fluctuation and a radial electric field fluctuation. The amplitude of the potential fluctuation is several hundred volts, and it is much larger than the potential fluctuation associated with turbulence-induced GAMs observed in the edge region in tokamak plasmas.

FIG.12 *Temperature dependence of the observed GAM frequency identified as an electrostatic potential fluctuation.*

Anomalous transport and losses of energetic ions caused by Alfvénic modes in NBI-heated plasmas have been studied with a scintillator-based lost fast ion probe (SLIP) and charge exchanged neutral particle analyzer. The m/n=1/1 toroidicity-induced Alfvén eigenmodes (TAEs) driven by co-going beam ions cause significant beam ion transport. Correlated with recurrent bursting TAEs, significant increases of energetic-ion losses are observed. Co-going transit energetic ions are responsible for destabilization of TAEs in LHD and are anomalously expelled through a diffusive-type loss mechanism. Figure 13 shows dependence of the increment of the energetic particle loss due to TAEs on the
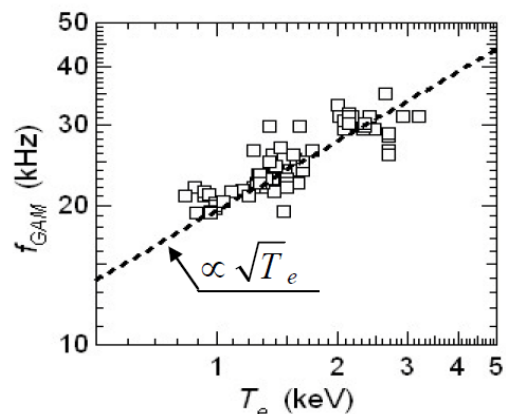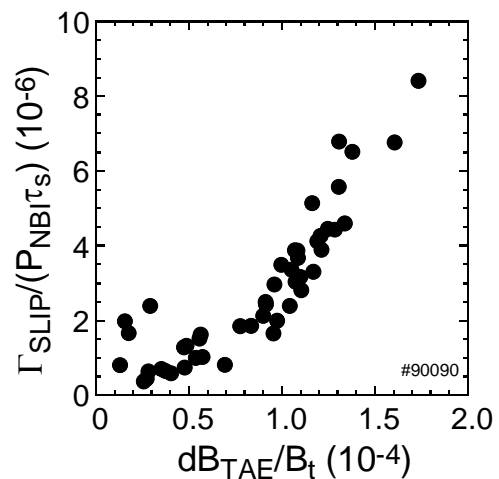

FIG.13 *Energetic-ion loss rate evaluated by the SLIP as a function of $\delta B_{TAE}/B_t$ at the Mirnov coil position. The ion loss is normalized by the beam pressure evaluated by the product of the heating power and the slowing down time τ_s.*

amplitude of the magnetic fluctuation burst. The increment of $\delta\Gamma_{\text{SLIP}}$ has a quadratic dependence on $\delta B_{TAE}/B_t$. The particle simulation with a modeled perturbed magnetic field suggests that energetic-ion losses increase as the amplitude of the perturbed field increases. Experimentally measured pitch-angle distributions of escaping beam ions are reproduced by this particle simulation.

5. Conclusions

The progress in physical understanding of net-current free helical plasmas in the LHD since the last Fusion Energy Conference in Geneva, 2008 is overviewed. The operational scenario has been explored in the extended high-density and high-β regimes. The maximum central density has reached $1.2 \times 10^{21}\text{m}^{-3}$ due to the formation of an IDB at the magnetic field of 2.5 T. The IDB has been maintained for 3 s by refueling with repetitive pellet injection [4]. The reactor-relevant β regime as high as 5 % has been investigated in detail to clarify the cause of the β limit in terms of magnetic geometry by the active magnetic axis scan [15]. The plasma with a central ion temperature reaching 5.6 keV exhibits the formation of an ITB. The ion thermal diffusivity decreases to the level predicted by neoclassical transport [7]. This ITB is accompanied by spontaneous toroidal rotation [7] and an *Impurity Hole* which generates an impurity-free core. A significant role of off-diagonal terms in transport is reflected in these remarkable features. *Impurity Hole* is found to be due to a large outward convection of impurities in spite of the negative radial electric field. The magnitude of the *Impurity Hole* is enhanced more in the magnetic configuration with larger helical ripple and for higher Z impurities [8]. Another mechanism to suppress impurity contamination has been identified in the edge plasma with stochastic magnetic fields. Impurity movement towards the downstream to divertor is enhanced in the high density operation [6]. The RMP has been used to clarify the physics issues related to induced magnetic island [16] and stochastic magnetic fields [17]. These issues range from the core to the edge in space and from MHD to transport in physics processes. It should be noted that the RMP facilitates the access to detachment through localization of radiation [5] and enhancement of density pump-out [4]. Non-local transport [12] and long-distance correlation [11] are new approaches to clarify the transport physics in toroidal plasmas. LHD is also a good experimental platform for the plasma wall interaction and in particular hydrogen retention has been assessed for the condition of the wall [21] including boronization [22].

In these days, the demand for 3-D modelling is becoming inevitable for accurate and detailed studies in tokamaks. Tokamaks and helical systems share common 3-D related physics issues such as documentation of 3-D equilibria, transport in a stochastic magnetic field, plasma response to RMP and divertor physics. Results from LHD would accelerate tokamak research in addition to advancing the prospect for a helical reactor.

References
[1]   KOMORI, A. et al., Fusion Sci. Tech. **58** (2010) 1.
[2]   YAMADA, H., et al., Fusion Sci. Tech. **58** (2010) 12.
[3]   KOMORI, A., et al., Nucl. Fusion **49** (2009) 104015.

[4]   MORISAKI, T., et al., "Progress of Superdense Plasma Research in LHD: Sustainment and Transport Study", EX/1-5 in this conference.

[5]   DRAPIKO, E.A., et al., "Effect of Magnetic Island on Three-Dimensional Structure of Edge Radation and Its Consequences for Detachment in LHD", EXD/P3-09 in this conference.

[6]   KOBAYASHI, M., et al., "Edge Impurity Transport Study in Stochastic Layer of LHD and Scrape-off Layer of HL-2A" EXD/6-5Ra in this conference.

[7]   NAGAOKA, K., et al., "Heat and Momentum Transport of Ion Internal Transport Barrier Plasmas on Large Helical Device", EXC/P4-08 in this conference.

[8]   YOSHINUMA, M., et al., "Impurity Transport of Ion ITB Plasmas on LHD", EX/9-1

[9]   SHIMIZU, A., et al., "Experimental Study of Potential Profile Formation in Large Helical Device", EXC/P4-11 in this conference.

[10] TAKAHASHI, H., et al., "High Electron Temperature Low Collisionality Plasma Confinement Characteristics in LHD", EXC/P8-15 in this conference.

[11] INAGAKI, S., et al., "Radial Structure of Fluctuation in Electron ITB Plasmas of LHD",EXC/7-4Ra in this conference.

[12] TAMURA, N., et al., "Edge-Core Interaction Revealed with Dynamic Transport Experiment in LHD", EXC/P8-16 in this conference.

[13] MASAMUNE, S., et al., "Mode Structure of Global MHD Instabilities and Its Effect on Plasma Confinement in LHD", EXS/P5-11 in this conference.

[14] FUNABA, H., et al. "Local Transport Property of Reactor-Relevant High-Beta Plasmas on LHD", EXC/P8-05 in this conference.

[15] SAKAKIBARA, S., et al., "Exploration of Optimal High-Beta Operation Regime by Magnetic Axis Swing in the Large Helical Device", EXS/P5-13 in this conference.

[16] NARUSHIMA, Y., et al., "Experimental Study of Poloidal Flow Effect on Magnetic Island Dynamics in LHD and TJ-II", EXS/P8-02 in this conference.

[17] IDA, K., et al., "Evidence of Stochastic Region near a Rational Surface in Core Plasmas of LHD", EX/5-2 in this conference.

[18] OSAKABE, M., et al., "Evaluation of Fast-Ion Confinement with Three Dimensional Magnetic Field Configurations on the Large Helical Device", EXW/P7-22 in this conference.

[19] ISOBE, M., et al., "Characteristics of Anomalous Transport and Losses of Energetic Ions Caused by Alfvénic Modes in LHD Plasmas", EXW/P7-09 in this conference.

[20] IDO, T., et al., "Potential Fluctuation Associated with Energetic-Particle Induced Geodestic Acoustic Mode in Reversed Magnetic Shear Plasmas on LHD", EXW/4-3Rb in this conference.

[21] HINO, T., et al., "Investigation of the Toroidal and Poloidal Dependences of First Wall Conditions in the Large Helical Device", EXD/P3-15 in this conference.

[22] OYA, Y., et al., "Impurity Effects on Hydrogen Isotope Retention in Boronized Wall of LHD", EXD/P3-25 in this conference.

[23] KITAJIMA, S., et al., "Electrode Biasing Experiment in the Large Helical Device", EXC/P8-07 in this conference.

[24] OHYABU, N., et al., Phys. Rev. Lett. **97** (2006) 055002.

[25] FENG, Y., et al., Contrib. Plasma Phys. **44** (2004) 57.

[26] REITER, D., et al., Fusion Sci. Technol. **47** (2005) 172.

[27] YOKOYAMA, M., et al., Nucl. Fusion **47** (2007) 1213.

[28] NARUSHIMA, Y., et al. Nucl. Fusion **48** (2008) 075010.